

# Combined piezoelectric and flexoelectric effects in resonant dynamics of nanocantilevers

Adriane G Moura and Alper Erturk 

*Journal of Intelligent Material Systems and Structures*

2018, Vol. 29(20) 3949–3959

© The Author(s) 2018

Article reuse guidelines:

sagepub.com/journals-permissions

DOI: 10.1177/1045389X18803441

journals.sagepub.com/home/jim



## Abstract

We establish and analyze an analytical framework by accounting for both the piezoelectric and flexoelectric effects in bimorph cantilevers. The focus is placed on the development of governing electroelastodynamic piezoelectric–flexoelectric equations for the problems of resonant energy harvesting, sensing, and actuation. The coupled governing equations are analyzed to obtain closed-form frequency response expressions via modal analysis. The combined piezoelectric–flexoelectric coupling coefficient expression is identified and its size dependence is explored. Specifically, a typical atomistic value of the flexoelectric constant for barium titanate is employed in the model simulations along with its piezoelectric constant from the existing literature. It is shown that the effective electromechanical coupling of a piezoelectric material, such as barium titanate, is significantly enhanced for thickness levels below 100 nm. The electromechanical coupling coefficient of a barium titanate bimorph cantilever increases from the bulk piezoelectric value of 0.065 to the combined piezoelectric–flexoelectric value exceeding 0.3 toward nanometer thickness level. Electromechanical frequency response functions for resonant power generation and dynamic actuation also capture the size-dependent enhancement of the electromechanical coupling. The analytical framework given here can be used for parameter identification and design of nanoscale cantilevers that can be used as energy harvesters, sensors, and actuators.

## Keywords

Piezoelectricity, flexoelectricity, energy harvesting, actuation, vibration

## Introduction

Piezoelectric coupling is defined by a third-rank tensor and is limited to certain materials that are non-centrosymmetric, ranging from natural quartz to man-made materials such as PZT (lead zirconate titanate) and BTO (barium titanate). Flexoelectricity, on the other hand, is the generation of electric polarization by the application of a non-uniform mechanical strain field, that is, a strain gradient (Maranganti and Sharma, 2009; Tagantsev et al., 2009; Yudin and Tagantsev, 2013). The phenomenon of flexoelectricity is a higher-order effect and is expected to be rather weak except for very small (submicron) dimensions, making the concept of interest mainly for microelectromechanical systems (MEMS) and especially nanoelectromechanical systems (NEMS) applications. Flexoelectricity is controlled by a fourth-rank tensor and is therefore allowed in materials of any symmetry. Therefore, any piezoelectric material also exhibits the flexoelectric effect at very low thickness levels, in the presence of non-homogeneous strain fields. As a gradient effect, flexoelectricity is size dependent, while piezoelectric coupling has no size dependence. Widely used

piezoelectric cantilever models developed for devices above micron-level thickness have to be modified for next-generation nanoscale devices since the effect of flexoelectric coupling will change the overall electroelastic dynamics at such small scales (Bhaskar et al., 2016).

Flexoelectric effect in solids has received suddenly growing attention especially after experiments by Ma and Cross (2001a, 2001b, 2002, 2003, 2005, 2006) on elastic dielectrics (Cross, 2006) and for potential small-scale applications thanks to developments in MEMS/NEMS. In addition to experimental efforts by Ma and Cross (Ma and Cross, 2001a, 2001b, 2002, 2003, 2005, 2006) and others (Huang et al., 2011; Zubko et al., 2007), mainly for samples with high dielectric constants, atomistic simulations (Maranganti and Sharma,

The Georgia W. Woodruff School of Mechanical Engineering, Georgia Institute of Technology, Atlanta, GA, USA

### Corresponding author:

Alper Erturk, The Georgia W. Woodruff School of Mechanical Engineering, Georgia Institute of Technology, Atlanta, GA 30332, USA.  
Email: alper.erturk@me.gatech.edu

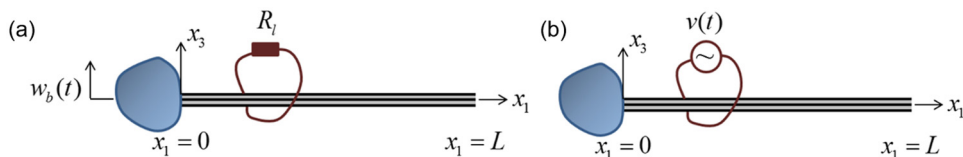


**Figure 1.** Bimorph cantilevers undergoing bending vibrations (exhibiting combined piezoelectric and flexoelectric effects at very small thickness levels): (a) energy harvesting/sensing in response to mechanical excitation and (b) shape morphing or dynamic actuation under electrical excitation. The piezoelectric layers are oppositely poled in the thickness direction (series connection) and the respective lateral faces have perfectly conductive and thin electrode layers.

2009) were presented to extract flexoelectric coefficients, and, importantly, substantial difference (several orders of magnitude) was reported between the simulated and identified flexoelectric coefficients (Cross, 2006). A comprehensive article on the flexoelectric effect in solids by Yudin and Tagantsev (2013) presents a detailed discussion on the subject matter along with a historical account. It is no surprise that with its promise of increased electromechanical coupling at small scales, flexoelectricity is of great interest for submicron level energy harvesting as well (Deng et al., 2014; Moura and Erturk, 2017).

In addition to the mismatch in the order of magnitude of flexoelectric coupling between atomistic simulations (Maranganti and Sharma, 2009) and experimental measurements (Cross, 2006), one of the issues in flexoelectric transduction and energy conversion has been the lack of a clear understanding and modeling of the converse effect, as the subject has created confusion since the converse effect is associated with a polarization gradient (Cross, 2006). For instance, it was suggested (Chu et al., 2009; Cross, 2006) that mechanical flexoelectric sensors could be made with no actuation property (which has no precedent or thermodynamic basis). In a recent effort for finite samples, Tagantsev and Yurkov (2012) presented a consistent and symmetric converse effect representation and its justification. Moura and Erturk (2017) implemented this converse coupling in a distributed-parameter electroelastic framework and showed the variation of the electromechanical coupling in centrosymmetric cantilevers for a broad thickness range, along with a case study on strontium titanate (STO) cantilevers. The present work aims to extend that effort to accommodate both piezoelectric and flexoelectric transduction mechanisms in piezoelectric materials such as BTO.

In the following, an analytical framework is developed and analyzed for combined transverse mode piezoelectric and flexoelectric effects in bimorph cantilevers for resonant energy harvesting and actuation. In addition to closed-form expressions for the electromechanically coupled voltage across the electrical load and the shunted vibration response, the combined piezoelectric and flexoelectric coupling coefficient is extracted and studied. A case study is used for

analyzing the energy harvesting and actuation performance, coupling coefficient, and size effects for a BTO bimorph cantilever under bending vibration using atomistic flexoelectric constant and bulk piezoelectric constant from the existing literature in the proposed framework.

### Direct and converse piezoelectric and flexoelectric effects

We consider the problem of a bimorph piezoelectric cantilever under bending vibrations as shown in Figure 1 for linear behavior (i.e. linear-elastic material behavior and geometrically small oscillations). The sample geometry justifies beam assumptions, such that the width ( $b$ ) and thickness ( $h$ ) of the rectangular cross-section are much shorter than the overhang length ( $L$ ). We further assume that the beam dimensions are such that the continuum theory is applicable (the beam length for the smallest case is orders of magnitude larger than the lattice parameter of the respective material). “Static” flexoelectricity (Yudin and Tagantsev, 2013) is applicable since the beam thickness (smallest dimension) is much smaller than the wavelength at vibration frequencies of interest. Assuming a linear constitutive behavior, polarization for combined direct piezoelectric and flexoelectric effects in the transverse mode can be written as

$$P_3 = \chi_{33}E_3 + e_{311}S_{11} + \mu_{1133} \frac{\partial S_{11}}{\partial x_3} \quad (1)$$

where  $P_3$  is the polarization in thickness direction (3-direction is the thickness direction and 1-direction is the axial direction in Figure 1),  $E_3$  is the electric field,  $S_{11}$  is the axial strain,  $\chi_{33}$  is the dielectric susceptibility,  $e_{311}$  is the piezoelectric constant, and  $\mu_{1133}$  is the flexoelectric coefficient.

The mechanical stress accounting for the converse piezoelectric and flexoelectric effects can be expressed as follows

$$T_{11} = c_{1111}S_{11} + e_{311}E_3 + f_{1133} \frac{\partial P_3}{\partial x_3} \quad (2)$$

or alternatively

$$T_{11} = c_{1111}S_{11} + e_{311}E_3 + \mu_{1133}\frac{\partial E_3}{\partial x_3} \quad (3)$$

where  $T_{11}$  is the axial stress,  $c_{1111}$  is the elastic modulus of the piezoelectric material (under short-circuit condition of the electrodes), and  $f_{1133}$  is the “flexocoupling coefficient” ( $f_{1133} = \chi_{33}^{-1}\mu_{1133}$ ). Note that the above form of flexoelectric coupling is suitable for basic “exogenous” strain gradients, such as those due to mechanical bending, but would be limited for “endogenous” ones, such as those due to domain boundaries and interfaces, which are beyond the scope of this work (Yudin and Tagantsev, 2013).

In the following, we develop and explore a complete analytical framework by accounting for both the piezoelectric and flexoelectric effects. The focus is placed on the development of governing electroelastodynamic piezoelectric–flexoelectric equations for the problems of energy harvesting, sensing, and actuation. The coupled governing equations are analyzed to obtain the frequency response functions such as the voltage output across the electrical load per base acceleration (in case of mechanical excitation) or electromechanical admittance in dynamic actuation (in case of electrical excitation). Furthermore, the coupling coefficient for the bimorph configuration is identified and its size dependence is explored.

### Euler–Bernoulli beam model for piezoelectric–flexoelectric energy harvesting and actuation

#### Coupled mechanical equation and modal analysis

The partial differential equation governing the forced vibration of a bimorph cantilevered piezoelectric thin beam under base excitation (Figure 1(a)) is

$$\begin{aligned} \frac{-\partial^2 M(x_1, t)}{\partial x_1^2} + c_s I \frac{\partial^5 w_{rel}(x_1, t)}{\partial x_1^4 \partial t} + c_a \frac{\partial w_{rel}(x_1, t)}{\partial t} \\ + m \frac{\partial^2 w_{rel}(x_1, t)}{\partial t^2} = -m \frac{d^2 w_b(t)}{dt^2} \end{aligned} \quad (4)$$

where  $w_{rel}(x_1, t)$  is the transverse displacement of the beam (neutral axis) relative to its base and  $M(x_1, t)$  is the internal bending moment at position  $x_1$  and time  $t$ ,  $c_a$  is the viscous air damping coefficient (mass proportional damping),  $c_s$  is the strain-rate damping coefficient (stiffness proportional damping),  $I$  is the second moment of area of the rectangular cross-section, and  $m$  is the mass per unit length of the beam ( $m = \rho b h = 2\rho b h_p$ , where  $b$  is the width of the beam,  $\rho$  is the mass density of the material,  $h_p$  is the thickness of each piezoelectric layer),  $h = 2h_p$  is the total beam thickness, and  $w_b(t)$  is the transverse displacement of the base. The linear damping coefficients employed in

equation (4) satisfy the proportional damping condition (Meirovitch, 2001) so that the corresponding undamped system’s mode shapes can be used in modal analysis.

The internal bending moment in equation (4) is the first moment of the axial stress field over the cross-section of each layer

$$M(x_1, t) = b \left( \int_{-h_p}^0 T_{11} x_3 dx_3 + \int_0^{h_p} T_{11} x_3 dx_3 \right) \quad (5)$$

The axial strain component is due to bending only and at a certain level ( $x_3$ ) from the neutral axis is proportional to the curvature of the beam

$$S_{11}(x_1, x_3, t) = -x_3 \frac{\partial^2 w_{rel}(x_1, t)}{\partial x_1^2} \quad (6)$$

and it is clear from equation (6) that the *strain gradient*  $\partial S_{11}/\partial x_3$  in this model is nothing but the *curvature* of the uniform Euler–Bernoulli beam (assuming the effect of the gradient  $\partial S_{11}/\partial x_1$  to be negligible).

Substituting equations (2) and (6) into the internal bending moment in equation (5) gives

$$\begin{aligned} M(x_1, t) = b \left( \int_{-h_p}^0 \left( c_{1111}^E S_{11} - e_{311} E_3 + f_{1133} \frac{\partial P_3}{\partial x_3} \right) x_3 dx_3 \right. \\ \left. + \int_0^{h_p} \left( c_{1111}^E S_{11} - e_{311} E_3 + f_{1133} \frac{\partial P_3}{\partial x_3} \right) x_3 dx_3 \right) \end{aligned} \quad (7)$$

For a finite sample (in which the polarization varies continuously from its bulk value to zero at the electrode boundaries (Tagantsev and Yurkov, 2012)), the flexoelectric term can be evaluated using integration by parts to identify the role of this term in the bending moment equation

$$\begin{aligned} b f_{1133} \left( \int_{-h_p}^0 \frac{\partial P_3}{\partial x_3} x_3 dx_3 + \int_0^{h_p} \frac{\partial P_3}{\partial x_3} x_3 dx_3 \right) \\ = -b f_{1133} \left( \int_{-h_p}^0 P_3 dx_3 + \int_0^{h_p} P_3 dx_3 \right) \\ = - (b f_{1133} h_p \langle P_3 \rangle + b f_{1133} h_p \langle P_3 \rangle) \end{aligned} \quad (8)$$

where  $\langle P_3 \rangle$  is the average polarization induced by the electric field in the beam. The spatial scale of the polarization variation at the interface is much smaller than the beam thickness; therefore,  $\langle P_3 \rangle \approx P$ , where the

polarization in the bulk (Tagantsev and Yurkov, 2012) can be given by

$$P = \chi_{33}E_3 \quad (9)$$

and it is useful to note from equations (2) and (3) that the dielectric susceptibility  $\chi_{33}$  is

$$\chi_{33} = \frac{\mu_{1133}}{f_{1133}} \quad (10)$$

The electric field component  $E_3$  should be expressed in terms of the respective voltage term for the series connection configuration shown in Figure 1(a). For the series connection of two oppositely poled identical piezoelectric layers, the voltage resultant is  $v(t)$ . It is important to note that for the series connection case,  $e_{311}$  has opposite signs for the top and bottom layers (due to opposite poling); therefore, the instantaneous electric fields are in the same direction (i.e.  $E_3 = -v(t)/2h_p$  in both layers) (Erturk and Inman, 2011).

The polarization in equation (9) can then be substituted into equation (8) along with the appropriate electric field equations for the series connection case. This gives the following contribution from the flexoelectric effect

$$-(bf_{1133}h_p\langle P_3 \rangle + bf_{1133}h_p\langle P_3 \rangle) = b\mu_{1133}v(t) \quad (11)$$

The flexoelectric and piezoelectric coupling terms resulting from equation (7) are only a function of time, and therefore, it must be multiplied by  $[H(x_1) - H(x_1 - L)]$  (where  $H(x_1)$  is the Heaviside function) to ensure its survival when the bending moment is substituted into equation (4). The internal bending moment is then

$$M(x_1, t) = -YI \frac{\partial^2 w_{rel}(x_1, t)}{\partial x_1^2} + \vartheta v(t)[H(x_1) - H(x_1 - L)] \quad (12)$$

where the coefficient of the backward coupling term ( $\vartheta$ ) for the series connection case is

$$\vartheta = \frac{1}{2}e_{311}bh_p + \mu_{1133}b \quad (13)$$

and the bending stiffness term  $YI$  of the composite cross-section (in short circuit) is

$$YI = \frac{2b}{3}c_{1111}h_p^3 \quad (14)$$

The coupled beam equation can then be obtained from equation (4) as

$$\begin{aligned} & YI \frac{\partial^4 w_{rel}(x_1, t)}{\partial x_1^4} + c_s I \frac{\partial^5 w_{rel}(x_1, t)}{\partial x_1^4 \partial t} + c_a \frac{\partial w_{rel}(x_1, t)}{\partial t} \\ & + m \frac{\partial^2 w_{rel}(x_1, t)}{\partial t^2} - \vartheta v(t) \left[ \frac{d\delta(x_1)}{dx_1} - \frac{d\delta(x_1 - L)}{dx_1} \right] \quad (15) \\ & = -m \frac{d^2 w_b(t)}{dt^2} \end{aligned}$$

where  $\delta(x_1)$  is the Dirac delta function that satisfies the following equation for a smooth test function  $\gamma(x_1)$

$$\int_{-\infty}^{\infty} \frac{d^{(n)}\delta(x_1 - p)}{dx_1^{(n)}} \gamma(x_1) dx_1 = (-1)^n \frac{d\gamma^{(n)}(p)}{dx_1^{(n)}} \quad (16)$$

The vibration response relative to the moving base can be expressed as

$$w_{rel}(x_1, t) = \sum_{r=1}^{\infty} \phi_r(x_1) \eta_r(t) \quad (17)$$

Here,  $\eta_r(t)$  is the modal mechanical coordinate and  $\phi_r(x_1)$  is the mass-normalized eigenfunction (obtained from the short-circuit problem) for the  $r$ th vibration mode for the series connection of the piezoelectric layers given by

$$\begin{aligned} \phi_r(x_1) &= \sqrt{\frac{1}{mL}} \\ & \left[ \cos \frac{\lambda_r}{L} x_1 - \cosh \frac{\lambda_r}{L} x_1 + \sigma_r \left( \sin \frac{\lambda_r}{L} x_1 - \sinh \frac{\lambda_r}{L} x_1 \right) \right] \quad (18) \end{aligned}$$

where  $\sigma_r$  is

$$\sigma_r = \frac{\sin \lambda_r - \sinh \lambda_r}{\cos \lambda_r + \cosh \lambda_r} \quad (19)$$

and the eigenvalues ( $\lambda_r > 0, r = 1, 2, \dots$ ) are the roots of the characteristic equation (for the short-circuit and clamped-free boundary conditions)

$$1 + \cos \lambda \cosh \lambda = 0 \quad (20)$$

The mass-normalized eigenfunctions in equation (17) satisfy the following orthogonality conditions

$$\int_0^L m \phi_r(x_1) \phi_s(x_1) dx_1 = \delta_{rs}, \quad \int_0^L YI \phi_r(x_1) \frac{d^4 \phi_s(x_1)}{dx_1^4} dx_1 = \delta_{rs} \omega_r^2 \quad (21)$$

where  $\delta_{rs}$  is the Kronecker delta and  $\omega_r$  is the undamped natural frequency of the  $r$ th vibration mode at short circuit ( $R_l \rightarrow 0$ )

$$\omega_r = \lambda_r^2 \sqrt{\frac{YI}{mL^4}} \tag{22}$$

The mechanical equation in modal coordinates can be obtained after substituting equation (17) into equation (15) (then multiplying the latter by the mode shape, integrating over the beam length, and applying orthogonality conditions) as

$$\frac{d^2 \eta_r(t)}{dt^2} + 2\zeta_r \omega_r \frac{d\eta_r(t)}{dt} + \omega_r^2 \eta_r(t) - \theta_r v(t) = f_r(t) \tag{23}$$

where the modal piezoelectric–flexoelectric electromechanical coupling term is

$$\theta_r = \vartheta \left. \frac{d\phi(x_1)}{dx_1} \right|_{x_1=L} = \left( \frac{1}{2} e_{311} b h_p + \mu_{1133} b \right) \left. \frac{d\phi(x_1)}{dx_1} \right|_{x_1=L} \tag{24}$$

and the modal mechanical forcing function can be expressed as

$$f_r(t) = -m \frac{d^2 w_b(t)}{dt^2} \int_0^L \phi_r(x_1) dx_1 \tag{25}$$

### Coupled electrical circuit equation and modal analysis

To derive the governing electrical circuit equations of the bimorph series configuration, we first examine a single layer under bending vibrations. The only source of mechanical strain is assumed to be the axial strain due to bending, yielding the following electric displacement  $D_3$

$$D_3 = \epsilon_{33} E_3 + e_{311} S_{11} + \mu_{1133} \frac{\partial S_{11}}{\partial x_3} \tag{26}$$

where  $\epsilon_{33}$  is the dielectric permittivity of the material,  $\epsilon_{33} = \epsilon_0 + \chi_{33} = (1 + \bar{\chi}_{33})\epsilon_0$  (note that for high- $K$  materials, which are of interest in flexoelectricity,  $\bar{\chi}_{33} \gg 1$ , and  $\epsilon_{33} \approx \chi_{33}$ ).

The piezoelectrically and flexoelectrically coupled electrical circuit equation can be obtained from

$$\frac{d}{dt} \left( \int_A \mathbf{D} \cdot \mathbf{n} dA \right) = \frac{v(t)}{R_l} \tag{27}$$

where  $\mathbf{D}$  is the vector of electric displacement components,  $\mathbf{n}$  is the unit outward normal of the electrodes, and the integration is performed over the electrode area  $A$ . The only contribution to the inner product of the integrand is from  $D_3$ . Using equation (26) in equation (27), the following circuit equation is obtained

$$\frac{\epsilon_{33} b L}{h_p} \frac{dv(t)}{dt} + \frac{v(t)}{R_l} + \left( \frac{1}{2} e_{311} h_p b + \mu_{1133} b \right) \int_0^L \frac{\partial^3 w_{rel}(x_1, t)}{\partial x_1^2 \partial t} dx_1 = 0 \tag{28}$$

which can be extended to the resultant of two layers in series connection (as in the case of a purely piezoelectric bimorph (Erturk and Inman, 2011)

$$C \frac{dv(t)}{dt} + \frac{v(t)}{R_l} + \sum_{r=1}^{\infty} \theta_r \frac{d\eta_r(t)}{dt} = 0 \tag{29}$$

where the modal electromechanical coupling is the same as equation (24), and the equivalent capacitance of two layers combined in series is

$$C = \frac{\epsilon_{33} b L}{2h_p} \tag{30}$$

Equations (23) and (29) are the governing electromechanical piezoelectric–flexoelectric bimorph cantilever equations in modal coordinates.

### Closed-form steady-state response in energy harvesting

For harmonic base excitation with  $w_b(t) = W_0 e^{j\omega t}$ , the modal forcing function given by equation (25) can be expressed as  $f_r(t) = F_r e^{j\omega t}$ , where the amplitude  $F_r$  is

$$F_r = \omega^2 m W_0 \int_0^L \phi_r(x_1) dx_1 \tag{31}$$

Then the steady-state modal mechanical response of the beam and the steady-state voltage response across the resistive load are also harmonic at the same frequency as  $\eta_r(t) = H_r e^{j\omega t}$  and  $v(t) = V e^{j\omega t}$ , respectively, where the amplitudes  $H_r$  and  $V$  are complexed values. Therefore, equations (23) and (29) yield

$$(\omega_r^2 - \omega^2 + j2\zeta_r \omega_r \omega) H_r - \theta_r V = F_r \tag{32}$$

$$\left( \frac{1}{R_l} + j\omega C \right) V + j\omega \sum_{r=1}^{\infty} \theta_r H_r = 0 \tag{33}$$

where  $\zeta_r$  is the modal mechanical damping ratio.

The steady-state voltage response is obtained as

$$v(t) = \frac{\sum_{r=1}^{\infty} \frac{-j\omega \theta_r F_r}{\omega_r^2 - \omega^2 + j2\zeta_r \omega_r \omega}}{\frac{1}{R_l} + j\omega C + \sum_{r=1}^{\infty} \frac{j\omega \theta_r^2}{\omega_r^2 - \omega^2 + j2\zeta_r \omega_r \omega}} e^{j\omega t} \tag{34}$$

Once the voltage across the electrical load is obtained, the current and power output can be calculated easily. For the case of a real-valued electrical load (i.e. a resistive load), the current delivered to the load is  $i(t) = v(t)/R_l$  and the instantaneous power output is  $P(t) = v^2(t)/R_l$ .

The steady-state modal mechanical response of the beam (that accounts for the converse piezoelectric–flexoelectric effect) can be obtained as

$$w_{rel}(x_1, t) = \sum_{r=1}^{\infty} \left[ \left( F_r - \theta_r \frac{\sum_{r=1}^{\infty} \frac{j\omega\theta_r F_r}{\omega_r^2 - \omega^2 + j2\zeta_r \omega_r \omega}}{\frac{1}{R_l} + j\omega C + \sum_{r=1}^{\infty} \frac{j\omega\theta_r^2}{\omega_r^2 - \omega^2 + j2\zeta_r \omega_r \omega}} \right) \frac{\phi_r(x_1) e^{j\omega t}}{\omega_r^2 - \omega^2 + j2\zeta_r \omega_r \omega} \right] \quad (35)$$

### Closed-form steady-state response in actuation

The governing equations in energy harvesting can be modified to represent the actuation problem, such that there is no base excitation ( $F_r = 0$ ), and the excitation is due to harmonic voltage input (Figure 1(b))

$$(\omega_r^2 - \omega^2 + j2\zeta_r \omega_r \omega) H_r = \theta_r V \quad (36)$$

$$-I + j\omega CV + j\omega \sum_{r=1}^{\infty} \theta_r H_r = 0 \quad (37)$$

where the  $V/R_l$  term is replaced with the current input  $-i(t) = -Ie^{j\omega t}$ . The steady-state mechanical response and actuation current are obtained by solving equations (36) and (37) as

$$w_{rel}(x_1, t) = \sum_{r=1}^{\infty} \frac{\theta_r \phi_r(x_1)}{\omega_r^2 - \omega^2 + j2\zeta_r \omega_r \omega} V e^{j\omega t} \quad (38)$$

$$i(t) = j\omega \left( C + \sum_{r=1}^{\infty} \frac{\theta_r^2}{\omega_r^2 - \omega^2 + j2\zeta_r \omega_r \omega} \right) V e^{j\omega t} \quad (39)$$

### Piezoelectric–flexoelectric electromechanical coupling coefficients and size effects

The electromechanical coupling coefficient  $k$  is a direct measure of energy conversion as commonly used in piezoelectricity (Lesieutre and Davis, 1997). A dynamic definition of the modal electromechanical coupling coefficient can be obtained based on the difference between the open-circuit and short-circuit natural frequencies (Lesieutre and Davis, 1997)

$$k^2 = \frac{(\omega_r^{oc})^2 - (\omega_r^{sc})^2}{(\omega_r^{oc})^2} \quad (40)$$

where  $k$  is the combined *piezoelectric–flexoelectric coupling coefficient* for the  $r$ th vibration mode (the focus in

the simulations of this work will be placed on the fundamental mode,  $r = 1$ ).

To express the coupling coefficient using equation (40), recall the undamped short-circuit natural frequency of the  $r$ th vibration mode

$$\omega_r^{sc} = \omega_r = \lambda_r^2 \sqrt{\frac{YI}{mL^4}} \quad (41)$$

Then, for modal vibrations under open-circuit conditions, equation (29) can be reduced to

$$v(t) = \frac{-\theta_r \eta_r(t)}{C}, R_l \rightarrow \infty \quad (42)$$

Substituting equation (42) into the modal mechanical equation of motion in equation (23), the undamped natural frequency of the  $r$ th vibration mode under open-circuit conditions becomes

$$(\omega_r^{oc})^2 = (\omega_r)^2 \left( 1 + \frac{\theta_r^2}{\omega_r^2 C} \right) \quad (43)$$

yielding

$$k^2 = \frac{\frac{\theta_r^2}{\omega_r^2 C}}{1 + \frac{\theta_r^2}{\omega_r^2 C}} = \frac{\theta_r^2}{\omega_r^2 C + \theta_r^2} = \frac{1}{1 + \frac{\omega_r^2 C}{\theta_r^2}} \quad (44)$$

Equation (44) can be simplified by substituting the expression for the equivalent capacitance and electro-mechanical coupling

$$k^2 = \frac{1}{1 + \frac{4e_{1111}^E \epsilon_{333}}{3\alpha_r^2 (\epsilon_{311} + 4\mu_{1133}/h)^2}} \quad (45)$$

where  $\alpha_r = -\sin \lambda_r - \sinh \lambda_r + \sigma_r (\cos \lambda_r - \cosh \lambda_r)$  and recall that  $h = 2h_p$ . Equation (45) clearly captures the thickness dependence of the flexoelectric effect and shows that with decreased thickness ( $h$ ), the coupling coefficient ( $k$ ) increases. This equation also shows the effect of material properties on the coupling coefficient and gives insight into the sign of the flexoelectric constant ( $\mu_{1133}$ ), which has been reported with different signs in the literature as pointed out by Zubko et al. (2013). According to equation (45), the flexoelectric and piezoelectric constants should have the same sign to prevent non-monotonic dependence of the coupling coefficient on the thickness (and its vanishing at a certain thickness value)—that is a negative  $e_{311}$  should be accompanied with a negative  $\mu_{1133}$ . It is worth

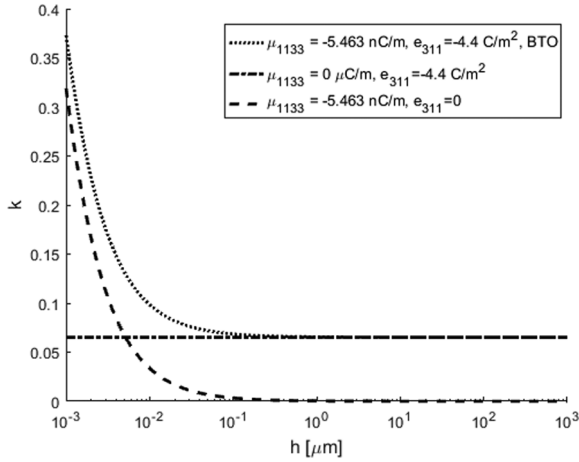


**Figure 2.** Transverse mode coupling coefficient ( $k$ ) versus bimorph thickness ( $h$ ) of a BTO cantilever for combined piezoelectric and flexoelectric, piezoelectric only, and flexoelectric only effects (for the first bending mode).

mentioning that the coupling coefficient depends on the vibration mode, electrode coverage, and so on. Typically, the first bending mode is of interest ( $r = 1$ ) for which full electrode coverage yields no charge cancellation.

## Case studies and results

### Electromechanical coupling and size effects

We consider BTO in our simulations using the atomistic value of  $\mu_{1133} = -5.463 \times 10^{-9} \text{ C/m}$  (Maranganti and Sharma, 2009). The electromechanical coupling coefficient due to combined piezoelectric and flexoelectric energy conversion is plotted for a range of cantilever thicknesses in Figure 2. The focus is placed on the fundamental bending vibration mode ( $r = 1$ ), and the beam thickness in the simulations ranges from 1 to 1 nm. As stated previously based on equation (45), the coupling coefficient increases with decreased thickness and is illustrated graphically in Figure 2. The isolated piezoelectric and flexoelectric coupling coefficients are also shown in this figure and it is seen that only for thickness levels below 100 nm does the flexoelectric effect become appreciable, and it strongly enhances the overall electromechanical coupling. For micron thickness levels and above, the overall electromechanical coupling is merely due to bulk piezoelectricity; however, the electromechanical coupling is dramatically enhanced due to flexoelectricity for thickness levels approaching the nanoscale.

### Resonant energy harvesting: electromechanical frequency response and size effects

The electromechanical frequency response behavior of a bimorph cantilevered piezoelectric and flexoelectric

energy harvester under base excitation is simulated with a focus on the first bending mode ( $r = 1$ ) for a range of electrical load resistive values. Three different geometric scales are explored ranging from millimeter scale to nanometer scale. The bimorph is made of BTO and has perfectly conductive surface electrodes on the faces that are perpendicular to the transverse base excitation (Figure 1). The atomistic value (Maranganti and Sharma, 2009) of  $\mu_{1133} = -5.463 \times 10^{-9} \text{ C/m}$  is used in the following simulations along with the necessary material properties (Bechmann, 1956):  $e_{311} = -4.4 \text{ C/m}^2$ ,  $c_{1111}^E = 166 \text{ GPa}$ ,  $\epsilon_{33}^s = 12.56 \text{ nF/m}$ , and  $\epsilon_{33}^E = 12.56 \text{ nF/m}$ . A mechanical quality factor ( $Q$ ) of  $\sim 50$  is assumed, yielding an approximate modal mechanical damping ratio of 1% of the critical damping for resonant vibrations. Three cases with total thicknesses ( $h$ ) of 1 mm, 1  $\mu\text{m}$ , and 1 nm (thickness of one layer of the bimorph is  $h_p = h/2$ ) are analyzed while keeping a constant aspect ratio of  $L/b/h$  fixed at 100/5/1. The mechanical excitation is harmonic base acceleration,  $d^2 w_b(t)/dt^2 = -\omega^2 W_0 e^{j\omega t}$ . Therefore, the results are presented as frequency response magnitude maps normalized by the base acceleration quantified in terms of gravitational acceleration ( $g = 9.81 \text{ m/s}^2$ ). To capture optimal load in power generation and respective trends with changing load, a range of electrical resistive load values spanning from short- to open-circuit conditions (100  $\Omega$  to 1 G $\Omega$ ) are simulated for each case.

The voltage output (per base acceleration) frequency response map for the 1-mm-thick BTO bimorph (100 mm  $\times$  5 mm  $\times$  1 mm) is shown in Figure 3(a). With increased electrical load resistance, the voltage increases monotonically at all frequencies, as a typical trend in energy harvesting (Erturk and Inman, 2011). It is shown that the resonance frequency for the 1-mm-thick STO cantilever is unaffected by the change in resistive load, that is, the frequency of peak magnitude does not change as the electrical load resistance value is swept from short- to open-circuit conditions. This indicates very low electromechanical coupling such that the feedback in the mechanical domain due to induced low voltage is negligible. The combined piezoelectric and flexoelectric coupling coefficient (for the 1 mm thickness level and BTO material properties) is obtained from equation (45) or Figure 2 as  $k = 0.0652$  (which is roughly the bulk piezoelectric value) confirming negligible contribution from flexoelectricity. The beam thickness is then decreased to 1  $\mu\text{m}$  while keeping the same aspect ratio (i.e. the dimensions are now 100  $\mu\text{m}$   $\times$  5  $\mu\text{m}$   $\times$  1  $\mu\text{m}$ ). The voltage output frequency response map for this case is shown in Figure 3(b). As with the 1 mm thickness case, the 1- $\mu\text{m}$ -thick BTO bimorph shows no noticeable shift in the fundamental resonance frequency with changing load resistance. The combined piezoelectric and flexoelectric coupling coefficient for this case is  $k = 0.0655$ , which, again,

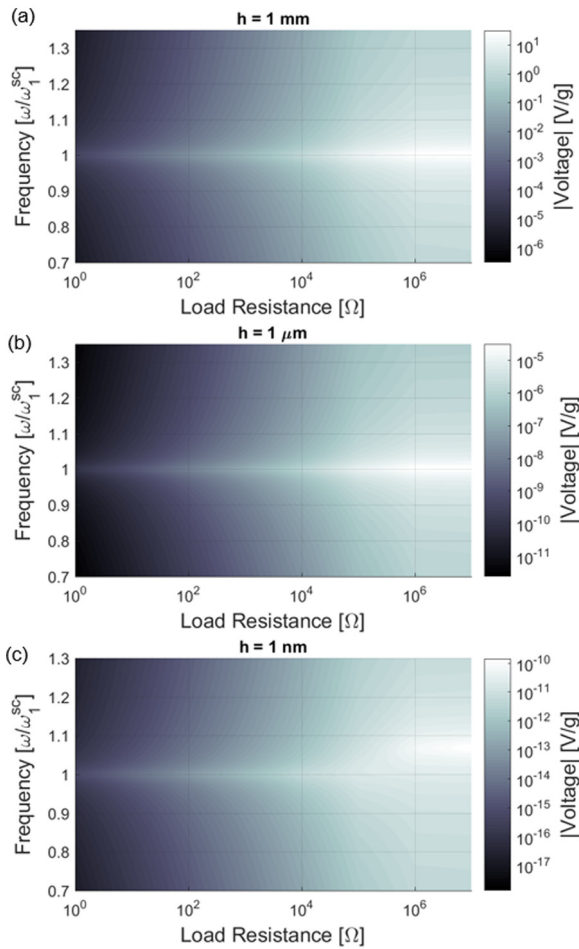


**Figure 3.** Voltage output frequency response versus load resistance maps (in magnitude form and per base acceleration) for cantilevered BTO harvesters with a fixed aspect ratio of 100/5/1 ( $L/b/h$ ) for three different geometric scales with the following thickness ( $h$ ) values: (a) 1 mm, (b) 1 μm, and (c) 1 nm.

indicates negligible flexoelectric contribution. The beam thickness is further decreased to 1 nm (beam dimensions of 100 nm × 5 nm × 1 nm) and the analysis is repeated. The nanometer-thick bimorph exhibits a shift in resonance from short- to open-circuit conditions, as shown in Figure 3(c). This shows significant electromechanical coupling as confirmed by the coupling coefficient of  $k = 0.365$  and Figure 2.

The electric current flowing to the resistive load is simply obtained from the voltage output using Ohm's law. The current output (per base acceleration) frequency response maps are also generated for the BTO bimorph for each geometric scale, as shown in Figure 4. The electrical current output decreases with increased electrical load resistance, which is the opposite trend as compared to voltage output. At all frequencies, the maximum current is achieved under short-circuit conditions of the surface electrodes. As

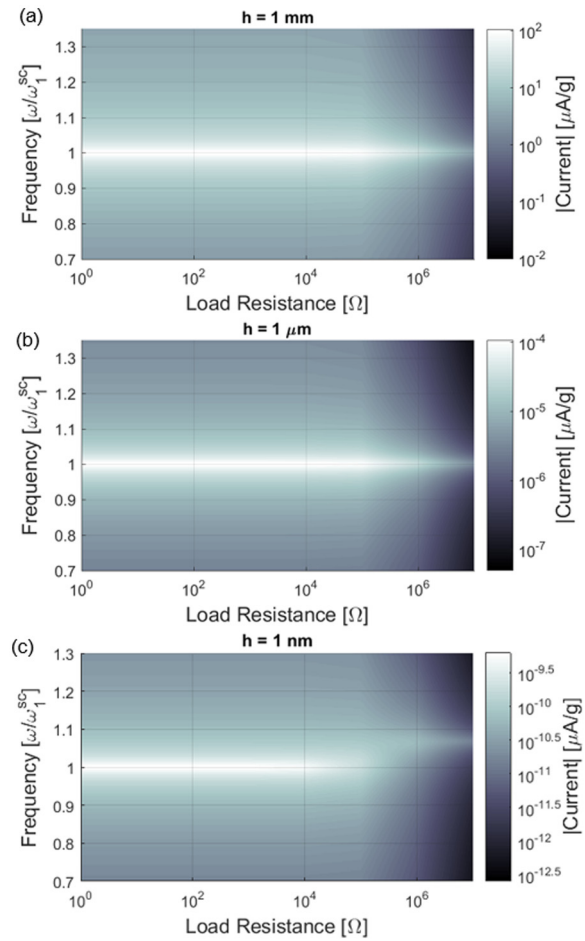


**Figure 4.** Current output frequency response versus load resistance maps (in magnitude form and per base acceleration) for cantilevered BTO harvesters with a fixed aspect ratio of 100/5/1 ( $L/b/h$ ) for three different geometric scales with the following thickness ( $h$ ) values: (a) 1 mm, (b) 1 μm, and (c) 1 nm.

with the voltage output frequency response maps, similar trends are observed for each case study in terms of the coupling coefficient. The thickness levels of 1 mm and 1 μm show no noticeable shift in resonance frequency (Figure 4(a) and (b)), indicating low electromechanical coupling. The 1 nm thickness case shows significant frequency shift (Figure 4(c)), revealing strong electromechanical coupling as discussed previously for the voltage output, as a result of flexoelectric contribution.

As a product of the two quantities which have opposite trends with changing load resistance, the electrical power exhibits more interesting trends, such as the presence of an optimal electrical load resulting in the maximum power output at a given frequency. The electrical power output is calculated for each of the three geometric scales with the fixed aspect ratio. The resulting graphs are shown in Figure 5. The optimal load for maximum power output can be determined for each case from the power output frequency response maps.

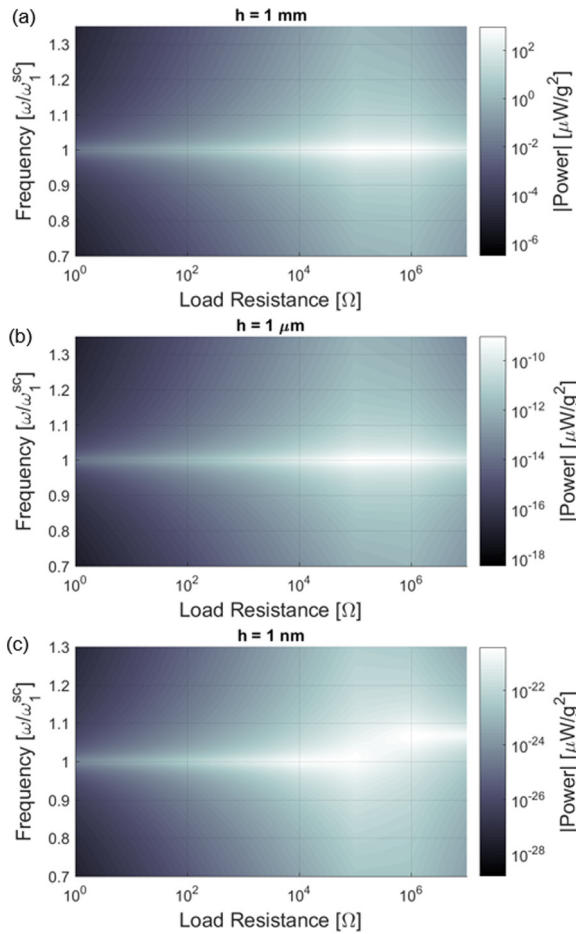


**Figure 5.** Power output frequency response versus load resistance maps (in magnitude form and per base acceleration) for cantilevered BTO harvesters with a fixed aspect ratio of 100/5/1 ( $L/b/h$ ) for three different geometric scales with the following thickness ( $h$ ) values: (a) 1 mm, (b) 1  $\mu\text{m}$ , and (c) 1 nm.

Both the 1 mm and 1- $\mu\text{m}$ -thick harvesters result in a peak power output around 100 k $\Omega$  (Figure 5(a) and (b)). As with the previous frequency response maps, the 1 mm and 1  $\mu\text{m}$  power output frequency response maps show the resonance frequency to be insensitive to the resistive load due to low electromechanical coupling. Consequently, a single optimal load is observed in the power map for the fundamental vibration mode for each case in Figure 5(a) and (b). However, the 1-nm-thick harvester exhibits two peak values for two distinct optimal electrical loads, 100 k $\Omega$  and 1 M $\Omega$ , respectively, at the short-circuit and open-circuit resonance frequencies, yielding the same power output (Figure 5(c)). This is an indication of a relatively strongly coupled harvester configuration, as a result of the electromechanical coupling enhancement due to the flexoelectric effect.

Finally, it is of interest to understand the structural response of the BTO bimorph while generating electricity from strain (piezoelectric effect) and strain gradient

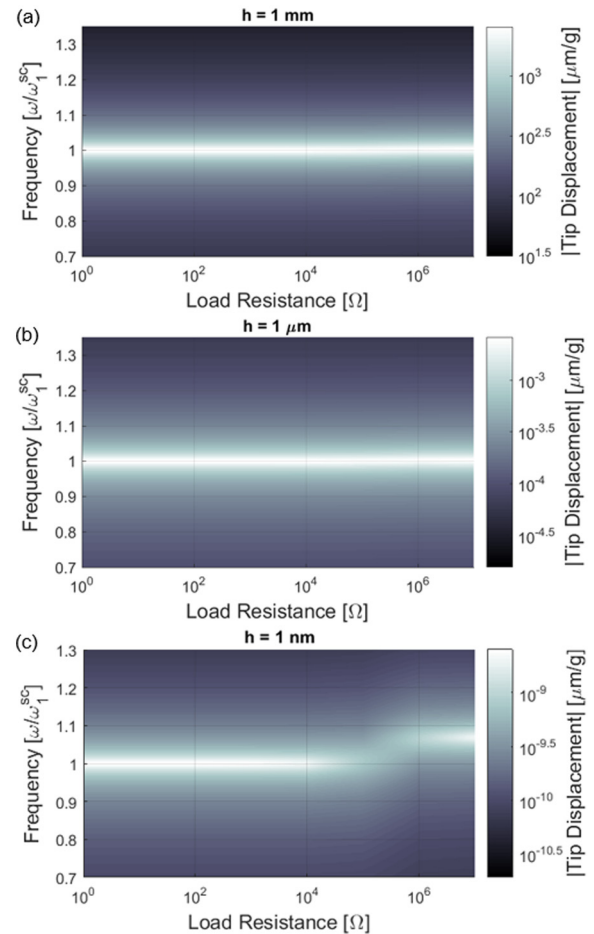


**Figure 6.** Tip displacement frequency response versus load resistance maps (in magnitude form and per base acceleration) for cantilevered BTO harvesters with a fixed aspect ratio of 100/5/1 ( $L/b/h$ ) for three different geometric scales with the following thickness ( $h$ ) values: (a) 1 mm, (b) 1  $\mu\text{m}$ , and (c) 1 nm.

(flexoelectric effect) fluctuations in response to mechanical base excitation. The motion of the cantilever is evaluated at the tip ( $x_1 = L$ ) using equation (35). Figure 6 shows the tip displacement maps for all three geometric scales of the bimorph using the same load resistances and normalized excitation frequency range. For the 1 mm and 1  $\mu\text{m}$ -thick bimorphs, the vibration responses of the cantilevers are insensitive to change in electrical load resistance, again, showing negligible electromechanical coupling at these thickness levels (Figure 6(a) and (b)). Therefore, as a result of weak electromechanical coupling, Joule heating in the resistive load does not create any significant dissipation in the vibration response of the BTO cantilever. However, for the bimorph with 1 nm thickness, the electromechanical coupling is relatively strong, as seen from previous electrical output graphs (Figures 3(c), 4(c), and 5c), and therefore, mechanical to electrical energy conversion is rather significant. Consequently, the structural response of the bimorph is sensitive to changing load

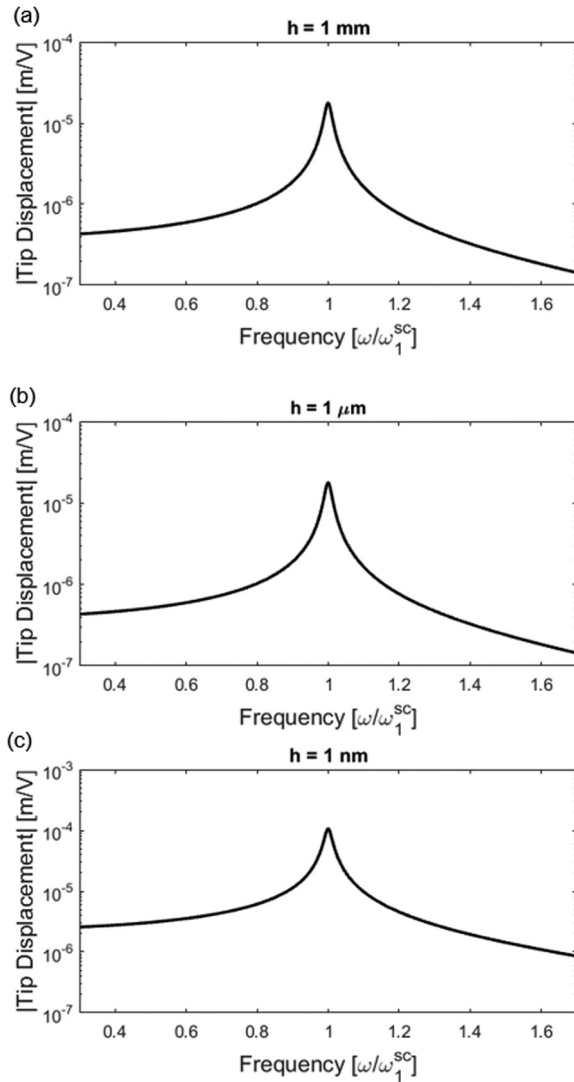


**Figure 7.** Tip displacement frequency response functions (in magnitude) for resonant actuation of BTO cantilevers with a fixed aspect ratio of 100/5/1 ( $L/b/h$ ) for three different geometric scales with the following thickness ( $h$ ) values: (a) 1 mm, (b) 1  $\mu\text{m}$ , and (c) 1 nm.

resistance near the resonant frequency (Figure 6(c)). Certain load resistance values result in significant shunt damping, confirming thermodynamic consistency of the fully coupled model.

### Resonant actuation: electromechanical frequency response and size effects

The same modeling framework is used to understand the electromechanical response of the bimorphs in the case of electrical excitation (voltage input) for the same set of system parameters. Of interest is the tip displacement frequency response (structural response for unit actuation voltage input) from equation (38) and the admittance frequency response (amount of current

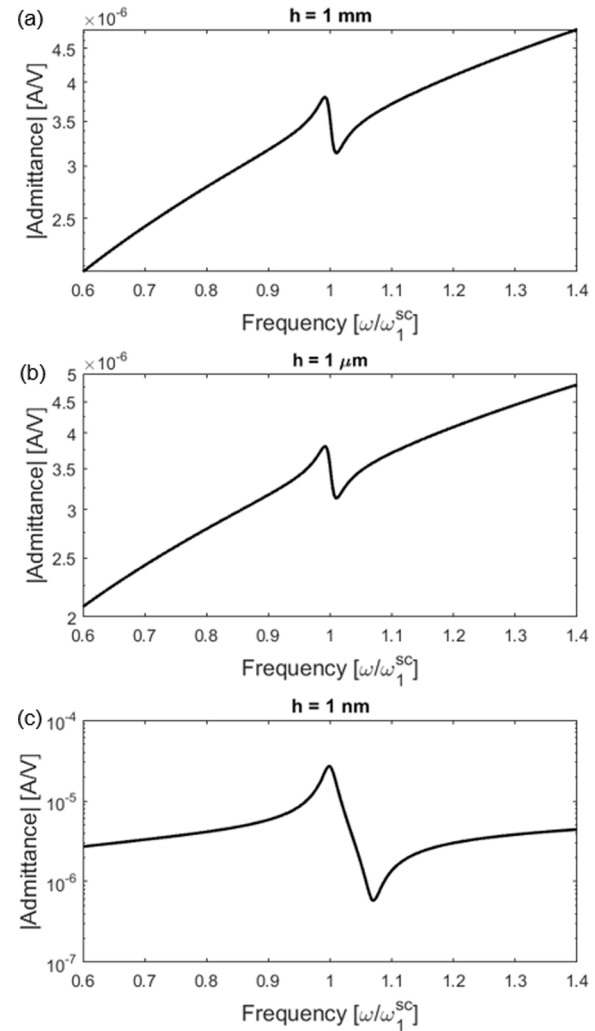


**Figure 8.** Admittance frequency response functions (in magnitude) for resonant actuation of BTO cantilevers with a fixed aspect ratio of 100/5/1 ( $L/b/h$ ) for three different geometric scales with the following thickness ( $h$ ) values: (a) 1 mm, (b) 1  $\mu\text{m}$ , and (c) 1 nm.

drawn for unit actuation voltage input) calculated from equation (39). The tip displacement and admittance frequency responses are shown in Figures 7 and 8, respectively. Particularly, in the admittance graphs shown in Figure 8, the relative frequency difference between the resonance and antiresonance frequencies is a measure of electromechanical coupling. These frequency response functions show, once again, that the overall coupling is enhanced due to flexoelectricity only at the nonometer scale.

### Conclusion

An electromechanical framework is developed and analyzed for combined transverse mode flexoelectric and piezoelectric energy harvesting as well as resonant actuation for the bending vibration of a piezoelectric

cantilever by accounting for two-way electromechanical coupling. The modeling framework is based on the Euler–Bernoulli beam theory and properly accounts for thermodynamically consistent, symmetric, direct, and converse coupling terms, and it captures the size effect on the combined flexoelectric–piezoelectric coupling coefficient. Based on a modal analysis procedure, closed-form solutions of the electromechanical frequency response functions are presented along with various case studies for a broad range of geometric parameters. Thickness dependence of the electromechanical coupling (which is a measure of energy conversion) is analytically extracted and its size dependence is observed also in simulations of the electromechanical frequency response functions. The flexoelectric–piezoelectric coupling increases from the bulk piezoelectric value of  $k = 0.0652$  at the millimeter scale to  $k = 0.365$  at the nanometer scale due to flexoelectric contribution. Overall, since the coupling coefficient is thickness dependent, the energy conversion dramatically increases in submicron thickness levels due to the flexoelectric effect. The proposed model can be used for parameter identification as well as performance quantification and optimization in combined flexoelectric and piezoelectric energy harvesting. The model was also implemented for dynamic actuation, which could be of interest for next-generation NEMS concepts involving actuation for nanocantilevers with submicron thickness levels.

### Declaration of conflicting interests

The author(s) declared no potential conflicts of interest with respect to the research, authorship, and/or publication of this article.

### Funding

The author(s) disclosed receipt of the following financial support for the research, authorship, and/or publication of this article: This work was supported by the National Science Foundation Grant CMMI-1463339, which is gratefully acknowledged.

### ORCID iD

Alper Erturk  <https://orcid.org/0000-0003-0110-5376>

### References

Bechmann R (1956) Elastic, piezoelectric, and dielectric constants of polarized barium titanate ceramics and some applications of the piezoelectric equations. *The Journal of the Acoustical Society of America* 28: 347–350.

Bhaskar UK, Banerjee N, Abdollahi A, et al. (2016) Flexoelectric MEMS: towards an electromechanical strain diode. *Nanoscale* 8: 1293–1298.

Chu B, Zhu W, Li N, et al. (2009) Flexure mode flexoelectric piezoelectric composites. *Journal of Applied Physics* 106: 104109.

Cross LE (2006) Flexoelectric effects: charge separation in insulating solids subjected to elastic strain gradients. *Journal of Materials Science* 41: 53–63.

Deng Q, Kammoun M, Erturk A, et al. (2014) Nanoscale flexoelectric energy harvesting. *International Journal of Solids and Structures* 51: 3218–3225.

Erturk A and Inman DJ (2011) *Piezoelectric Energy Harvesting*. Chichester: Wiley.

Huang W, Kim K, Zhang S, et al. (2011) Scaling effect of flexoelectric (Ba, Sr)TiO<sub>3</sub> microcantilevers. *Physica Status Solidi (RRL)–Rapid Research Letters* 5: 350–352.

Lesieutre GA and Davis CL (1997) Can a coupling coefficient of a piezoelectric device be higher than those of its active material? *Journal of Intelligent Material Systems and Structures* 8: 859–867.

Ma W and Cross LE (2001a) Large flexoelectric polarization in ceramic lead magnesium niobate. *Applied Physics Letters* 79: 4420–4422.

Ma WH and Cross LE (2001b) Observation of the flexoelectric effect in relaxor Pb(Mg<sub>1/3</sub>Nb<sub>2/3</sub>)O<sub>3</sub> ceramics. *Applied Physics Letters* 78: 2920–2921.

Ma WH and Cross LE (2002) Flexoelectric polarization of barium strontium titanate in the paraelectric state. *Applied Physics Letters* 81: 3440–3442.

Ma WH and Cross LE (2003) Strain-gradient-induced electric polarization in lead zirconate titanate ceramics. *Applied Physics Letters* 82: 3293–3295.

Ma WH and Cross LE (2005) Flexoelectric effect in ceramic lead zirconate titanate. *Applied Physics Letters* 86: 072905.

Ma WH and Cross LE (2006) Flexoelectricity of barium titanate. *Applied Physics Letters* 88: 232902.

Maranganti R and Sharma P (2009) Atomistic determination of flexoelectric properties of crystalline dielectrics. *Physical Review B* 80: 054109.

Meirovitch L (2001) *Fundamentals of Vibrations*. New York: McGraw-Hill.

Moura AG and Erturk A (2017) Electroelastodynamics of flexoelectric energy conversion and harvesting in elastic dielectrics. *Journal of Applied Physics* 121: 064110.

Tagantsev AK and Yurkov AS (2012) Flexoelectric effect in finite samples. *Journal of Applied Physics* 112: 044103.

Tagantsev AK, Meunier V and Sharma P (2009) Novel electromechanical phenomena at the nanoscale: phenomenological theory and atomistic modeling. *MRS Bulletin* 34: 643–647.

Yudin P and Tagantsev A (2013) Fundamentals of flexoelectricity in solids. *Nanotechnology* 24: 432001.

Zubko P, Catalan G and Tagantsev AK (2013) Flexoelectric effect in solids. *Annual Review of Materials Research* 43: 387–421.

Zubko P, Catalan G, Buckley A, et al. (2007) Strain-gradient-induced polarization in SrTiO<sub>3</sub> single crystals. *Physical Review Letters* 99: 167601.